frontiers in Marine Science

ORIGINAL RESEARCH
published: 04 February 2019
doi: 10.3389/fmars.2019.00011

Oxygen Profiles Across the Sea-Surface Microlayer—Effects of Diffusion and Biological Activity

Janina Rahlff[1†‡], Christian Stolle[1,2*†], Helge-Ansgar Giebel[3], Mariana Ribas-Ribas[1], Lars Riis Damgaard[4] and Oliver Wurl[1]*

[1] Center for Marine Sensors, Institute for Chemistry and Biology of the Marine Environment, Carl-von-Ossietzky University Oldenburg, Wilhelmshaven, Germany, [2] Leibniz-Institute for Baltic Sea Research Warnemuende, Rostock, Germany, [3] Institute for Chemistry and Biology of the Marine Environment, Carl-von-Ossietzky University Oldenburg, Oldenburg, Germany, [4] Section for Microbiology, Department of Bioscience, Aarhus University, Aarhus, Denmark

OPEN ACCESS

Edited by:
Marta Álvarez, Instituto Español de Oceanografía (IEO), Spain

Reviewed by:
Wei-dong Zhai, Shandong University (Qingdao), China
Jesus M. Arrieta, Centro Oceanográfico de Canarias, Instituto Español de Oceanografía (IEO), Spain

***Correspondence:**
Janina Rahlff
janina.rahlff@uni-oldenburg.de
Christian Stolle
christian.stolle2@uni-oldenburg.de

†These authors have contributed equally to this work

‡Present Address:
Janina Rahlff, Group for Aquatic Microbial Ecology, Biofilm Centre, University of Duisburg-Essen, Essen, Germany

Specialty section:
This article was submitted to Marine Biogeochemistry, a section of the journal Frontiers in Marine Science

Received: *09 February 2018*
Accepted: *14 January 2019*
Published: *04 February 2019*

Citation:
Rahlff J, Stolle C, Giebel H-A, Ribas-Ribas M, Damgaard LR and Wurl O (2019) Oxygen Profiles Across the Sea-Surface Microlayer—Effects of Diffusion and Biological Activity. Front. Mar. Sci. 6:11. doi: 10.3389/fmars.2019.00011

Gas exchange across the air-water interface is strongly influenced by the uppermost water layer (<1 mm), the sea-surface microlayer (SML). However, a clear understanding about how the distinct physicochemical and biological properties of the SML affect gas exchange is lacking. We used an automatic microprofiler with Clark-type microsensors to measure small-scale profiles of dissolved oxygen in the upper 5 cm of the water column in a laboratory tank filled with natural seawater. We aimed to link changing oxygen concentrations and profiles with the metabolic activity of plankton and neuston, i.e., SML-dwelling organisms, in our artificial, low-turbulence set-up during diel cycles. We observed that temporal changes of the oxygen concentration in near surface water (5 cm depth) could not be explained by diffusive loss of oxygen, but by planktonic activity. Interestingly, no influence of strong neuston activity on oxygen gradients at the air-water interface was detectable. This could be confirmed by a modeling approach, which revealed that neuston metabolic activity was insufficient to create distinct curvatures into these oxygen gradients. Moreover, the high neuston activity in our study contributed only ≤7.1% (see **Supplementary Table 4**) to changes in oxygen concentration in the tank. Overall, this work shows that temporal and vertical variation of oxygen profiles across the air-water interface in controlled laboratory set-ups is driven by biological processes in the underlying bulk water, with negligible effects of neuston activity.

Keywords: oxygen gradients, sea-surface microlayer, microsensors, net community production, gas exchange, neuston, plankton, diffusion

INTRODUCTION

The sea-surface microlayer (SML) forms a boundary layer at the air-water interface, which has distinct physicochemical and biological properties compared to the underlying water (ULW) (Hardy, 1982; Wurl et al., 2017). The SML was historically considered as multiple layers with lipids accumulating on top of the air-water interface (Hardy, 1982), but this conceptual model was challenged by the idea of the SML rather being a gelatinous matrix (Sieburth, 1983). Independent of its composition, the vertical dimension of the SML is still unclear and its thickness is vaguely defined to be <1 mm (Liss and Duce, 2005). Due to its position between the atmosphere and hydrosphere, the SML has profound implications in air-sea interaction, such as the exchange of climate-relevant gases (Frew, 1997). Organic surface-active substances, i.e., surfactants, accumulate in the SML

(Wurl et al., 2011b) even at wind speeds up to 13 m s^{-1} in the Atlantic Ocean (Sabbaghzadeh et al., 2017). The SML constitutes a demanding habitat for its colonizing organisms, termed as neuston (Naumann, 1917). Microbial activity and community composition in the SML are affected by harsh meteorological conditions such as ultra-violet (UV) radiation (Agogué et al., 2005; Santos et al., 2012) and the turbulence resulting from wind speed (Stolle et al., 2011; Rahlff et al., 2017a). Within the SML, microbial heterotrophic metabolism is often enhanced compared to the ULW (Obernosterer et al., 2005; Reinthaler et al., 2008). This is most likely driven by the strong accumulation of organic matter within a gelatinous matrix (Cunliffe et al., 2013). Even though it has been observed that photosynthetic activity in the SML may be inhibited by high light intensities (Albright, 1980; Hardy and Apts, 1984), strong enrichments of phytoneuston may occur, for instance in sheltered bays and lagoons (Hardy, 1973), in foams (Maynard, 1968), and in association with surface slicks (Sieburth and Conover, 1965; Carlson, 1982b; Wurl et al., 2016).

Generally, air-sea gas exchange may be influenced by neuston communities in two ways. First, the neuston may modulate the quantity or composition of surfactants in the SML being produced by planktonic organisms (Žutić et al., 1981; Satpute et al., 2010). Surfactants form a laminar diffusion layer and reduce gas transfer velocities (Goldman et al., 1988; Frew et al., 1990). Secondly, the neuston metabolizes gases directly, e.g., methane (Upstill-Goddard et al., 2003) and carbon monoxide (Conrad and Seiler, 1988). Functional gene analysis indicated that different methanotrophic bacterial communities in the SML and ULW (Cunliffe et al., 2008) may be involved in gas turnover in these two habitats. Calleja et al. (2005) found that net heterotrophic activity in the top 2 cm of the ocean contributed to carbon dioxide (CO_2) emissions at some stations of the subtropical Atlantic Ocean. However, the authors also observed at other stations that autotrophic organisms contributed to an under-saturation of CO_2 in the water and hence increased its uptake from the atmosphere. Calleja et al. (2013) provided first evidence, that the partial pressure of CO_2 (pCO_2) is vertically inhomogeneous from few cm below the air-water interface to 5 m water depth, probably changing estimates on the magnitude and the direction of air-sea CO_2 flux. These studies strongly underline the need for further research on the temporal and spatial variability of gas profiles in surface water including the SML and their dependencies on biological activity.

Clark-type microsensors are used in a broad range of applications in oceanographic and limnologic research (Revsbech, 1989), especially in microbial ecology (Revsbech and Jørgensen, 1986). For instance, oxygen (O_2) microsensors were applied to determine bacterial growth efficiency in aquatic ecosystems by measuring respiration rates (Ploug and Grossart, 1999; Briand et al., 2004). In addition, microsensors have been successfully used to record O_2 microprofiles, for instance to explore the vertical distribution of photosynthetic activity within microbial mats (Revsbech et al., 1983), in cyanobacterial surface aggregates (Ploug, 2008) as well as in single *Trichodesmium* colonies (Eichner et al., 2017). Microsensors have also been applied to determine the thickness of the SML (Zhang et al., 2003).

In this study, we used microsensors for high resolution measurements to investigate temporal changes of O_2 profiles across the air-water interface and to link those with biological O_2 turnover within the SML. Our study presents highly-resolved vertical (50–500 μm-steps) O_2 and temperature profiles across the SML into the ULW to a depth of 5 cm in a tank filled with natural seawater. We investigated whether temporal, i.e., diel and thus light-dependent changes in O_2 concentration at this depth are related to net community production (NCP) in SML (neuston) and ULW (plankton).

MATERIALS AND METHODS

Experimental Set-Up

Seawater from the Jade Bay (North Sea) offshore the city Wilhelmshaven (Germany, 53°30′50.0″N 8°08′44.2″E) was pumped on 6th July 2016 at high tide from a depth of ∼1–2 m into an outside basin to allow settlement of sediment particles for 5 days. This water was used for both of the following experiments. On 11th July 2016, water from the outside basin was filtered through a 100 μm mesh and filled into a ∼700-L aquarium tank (2.2 × 0.6 × 0.5 m), made from glass. The first experiment ran from July 13–18th 2016 (Day 1–6). On 19th July 2016, the tank was refilled with water from the outside basin for a second experiment that ran from July 20th−22nd 2016 (Day 1–3). The open tank was placed in a greenhouse, which allowed exposure to diel light changes. Air (in the greenhouse) and water temperature in the tank varied from 17 to 30°C and from 20 to 26°C, respectively. Photosynthetically active radiation (PAR) was recorded using the Quantum Meter MQ-200 (Apogee Instruments, UT, USA) in a wavelength range of 410–655 nm. The PAR sensor was attached 1 m above the water surface. PAR data were measured every 30 s, and the mean of 60 measurements was logged every 30 min. For relationships between PAR and NCP, the mean PAR for the duration of each NCP incubation period (**Table 1**) was calculated. All dates and times mentioned throughout this work refer to UTC +01:00. The experimental set-up is illustrated in **Supplementary Figure 1**.

Measurement of O_2 and Temperature Profiles

Microprofiles of O_2 and temperature in the laboratory tank were simultaneously measured using a Clark-type O_2 microsensor OX-50 and a temperature microsensor TP-200 (Unisense, Denmark), respectively, which were connected to an amplifier (Multimeter, Unisense, Denmark). The response times for OX-50 and TP-200 are <5 and <3 s, respectively. Profiles were measured using the MicroProfiling system (Unisense, Denmark), i.e., a motorized micromanipulator that was installed on top of the aquarium tank and controlled by a computer (**Supplementary Figure 1**). Signals were recorded using the software SensorTraceSuite (Version 2.6.100). The temperature sensor was calibrated each day to three random temperatures within the ranges of 0–10, 10–30, and 30–50°C measured with a mercury thermometer. The O_2 microsensor was calibrated with two points using an anoxic 0.1 M sodium ascorbate solution for 0% standard. The signal of 100% air-saturated water was

TABLE 1 | Absolute data and rate calculations for temporal changes of oxygen, temperature, net community production (NCP), photosynthetically active radiation (PAR), and diffusive fluxes between profiles.

Exp	Date of t_0	Time point[a]	Temporal changes between profiles (absolute)			Temporal changes between profiles (normalized)		Net community production[b]				Mean PAR[f]	Mean diffusive flux
			O_2	Temperature	Time	O_2	Temperature	SML_01	SML_02	ULW_01	ULW_02		
			(μmol O_2 L^{-1})	(°C)	(h)	(μmol O_2 L^{-1} h^{-1})	(°C h^{-1})	(μmol O_2 L^{-1} h^{-1})	(μmol O_2 L^{-1} h^{-1})	(μmol O_2 L^{-1} h^{-1})	(μmol O_2 L^{-1} h^{-1})	(μmol m^{-2} s^{-1})	(μmol O_2 L^{-1} h^{-1})
1	13 July 2016	t_1-t_0	−17.51	−0.64	14.94	−1.17	−0.04	1.83	4.51	2.66	3.04	62.87	−0.22
		t_{end}-t_1	12.88	−0.08	5.76	2.24	−0.01	24.31[c]		−7.94		98.45	−0.23
		t_{end}-t_0	−4.63	−0.72	20.70	−0.22	−0.04	7.89		−0.01		70.27	−0.37
1	14 July 2016	t_1-t_0	−16.05	−1.01	15.50	−1.04	−0.07	−15.77	−21.30	−1.06	−1.28	30.49	−0.20
		t_{end}-t_1	−8.11	2.05	31.54	−0.26	0.06	12.85	16.83	−0.18	0.05	65.45	−0.08
		t_{end}-t_0	−24.16	1.04	47.04	−0.51	0.02	2.68	3.74	−0.48	−0.44	51.18	−0.27
1	15 July 2016	t_1-t_0	14.20	1.38	11.45	1.24	0.12	44.78	41.77	1.97	0.79	120.36	−0.22
		t_{end}-t_1	−19.09	0.38	15.73	−1.21	0.02	−14.82	−10.41	−1.42	−1.18	29.41	−0.29
		t_{end}-t_0	−4.89	1.76	27.18	−0.18	0.06	7.58	8.82	−0.28	−0.47	66.20	−0.09
2	20 July 2016	t_1-t_0	−24.37	0.73	5.02	−3.72	0.15	−4.00	−6.02	−1.80	−1.59	232.50	−0.55
		t_2-t_1	8.79	0.66	3.91	0.79	0.17	−6.77	−6.29	−2.02[d]	−2.35	39.11	−0.58
		t_3-t_2	−10.36	−0.15	5.26	−1.97	−0.03	−13.96	−13.40	−1.32[e]	−2.61	1.27	−0.49
		t_4-t_3	−13.84	−0.18	2.98	−4.64	−0.06	−14.15	−14.53	−3.97	−3.02	0.00	−0.37
		t_5-t_4	−7.58	−0.22	3.85	−1.97	−0.06			−1.28	−1.46	10.29	−0.22
		t_6-t_5	−17.97	0.89	5.63	−3.19	0.16			−0.74	−0.63	157.44	−0.07
		t_{end}-t_6	1.55	0.15	3.23	0.48	0.05			−1.18	−1.47	132.50	−0.06
		t_{end}-t_0	−63.77	1.87	29.88	−2.13	0.06			−2.29	−2.46	89.00	−0.30
2	21 July 2016	t_{end}-t_0	−22.12	−1.21	21.71	−1.02	−0.06			−2.02	−2.15	38.59	0.09

[a]*see* ***Supplementary Table 1*** *for detailed date and time of the incubation and profiling,* [b]*error propagation of standard errors for the mean was always < 0.2 μmol O_2 L^{-1} h^{-1} except for* [c]*0.53 μmol O_2 L^{-1} h^{-1},* [d]*0.44 μmol O_2 L^{-1} h^{-1},* [e]*0.35 μmol O_2 L^{-1} h^{-1},* [f]*mean values for the duration of the incubation time/time between profiles.*

taken from the 0 μm water depth (i.e., the air-water interface) of each individual profile, assuming 100% air-saturation due to equilibration with the atmosphere. The 0 μm water depth and its corresponding signal value was established for each profile as the crossing point between (a) the regression line through the approximately constant O_2 sensor values in air and (b) the regression line through the data points in the first 500 μm that deviated from the air values (**Supplementary Figure 2**). To reduce ambiguity, the first three data points on the airside and the waterside of the air-water interface were excluded for regression analyses. The value at 0 μm depth was converted into μmol O_2 L^{-1} using the salinity and temperature dependent O_2 solubility (Garcia and Gordon, 1992).

To account for different vertical resolution, profiles were measured in seawater of the tank either in vertical steps of 50 μm to a depth of 5 mm (shallow profile) or in 500 μm steps to a depth of 5 cm (deep profile) through the SML in direction from air to water.

Temperature-Correction of O_2 Gradients

The O_2 microsensor was recalibrated at the temperature, which was measured at 0 μm water depth. As described above, the 0 μm water depth was defined by the intersecting linear regression lines of air and water temperature readings. To account for minor vertical changes of the water temperature in the tank within the upper centimeters (**Supplementary Figure 3**), the O_2 profile data was temperature-corrected for each individual depth according to Rahlff et al. (2017b) and Unisense supportive material.

Dynamics of O_2 Concentrations in the Tank and Diffusive Losses

To determine the O_2 concentration in the ULW, the mean O_2 concentration was calculated using data from the deep O_2 profiles from 1.5 to 4.0 cm water depth. To describe the temporal variability of the mean O_2 concentration, the differences between two deep profiles were calculated and expressed in μmol O_2 L^{-1} h^{-1}. The analyzed profiles corresponded to the time points t_0, t_n, and t_{end} of the incubation experiments (**Table 1** and **Supplementary Table 1**) to allow for direct comparison with metabolic activity.

For calculation of O_2 losses from the tank by diffusion we considered the Whitman film model, which describes molecular diffusion through a stagnant, laminar layer (Gladyshev, 2002). Diffusive rates (μmol L^{-1} h^{-1}) were calculated for each O_2 gradient as follows:

$$Diffusive\ rate\ (\mu mol\ L^{-1}h^{-1}) = DS\frac{1}{V}\left(C_0 - C_{ULW}\right)\frac{1}{\delta} \quad (1)$$

where D is the diffusion coefficient (cm^2 h^{-1}) obtained from a straight line equation of D vs. temperature (Ramsing and Gundersen, 2000) at a salinity of 30. The mean temperature within the upper 1.1 mm [defined as the diffusive boundary layer (DBL)] was calculated from each profile to be analyzed. S is the surface area of the aquarium (12,490 cm^2), V is the tank volume (673.2 L), δ is the thickness of the SML, which we considered to be the thickness of the DBL (1.1 mm) as deduced from all O_2 gradients measured. C_0 is the O_2 concentration (μmol L^{-1} h^{-1}) at the interface (0 μm) and C_{ULW} is the O_2 concentration at 1.1 mm water depth.

Finally, we calculated the mean diffusive rate from the diffusive rates of two shallow profiles, which were recorded in temporal proximity to the deep profiles that in turn were used to calculate the mean O_2 concentration.

Profile Model

To evaluate the theoretical effect of biological metabolism (i.e., NCP) on O_2 profiles in the SML, we used a simple mathematical steady-state model with the assumption of a stagnant, homogeneous SML bordering sharply to a well-mixed ULW with constant concentrations (**Figure 1**). At steady state, a modified version of Fick's 2nd Law describes the concentration $C_R(x)$ of a substance, which is both diffusing and reacting (consumption or production) as a function of depth x as

$$D\frac{d^2C_R(x)}{dx^2} = -R \quad (2)$$

Where D is the diffusion coefficient and R is the constant reaction rate (positive for production and negative for consumption) for the gas. Integrating this equation with the boundary conditions that the concentration at the top (depth = 0 μm) of the SML, C_0, is constant at equilibration with the atmosphere and the concentration at the bottom (depth = l) of the SML, C_{ULW}, is constant and equal to the ULW concentration, yields the concentration profile in the SML as a function of depth x (**Figure 1**):

$$C_R(x) = C_0 - \frac{R}{2D}x^2 + \frac{C_{ULW} - C_0 + \frac{R}{2D}l^2}{l}x \quad (3)$$

If the reaction rate is zero, the concentration profile, $C_{NR}(x)$, becomes

$$C_{NR}(x) = C_0 + \frac{C_{ULW} - C_0}{l}x \quad (4)$$

and the difference between the concentration profile with and without reaction is thus

$$C_R(x) - C_{NR}(x) = -\frac{R}{2D}x^2 + \frac{R}{2D}lx \quad (5)$$

This difference is a parabola with its maximum/minimum at

$$x = \frac{l}{2} \quad (6)$$

i.e., in the middle of the SML, where the value of this absolute difference is

$$diff_{max} = \frac{Rl^2}{8D} \quad (7)$$

The value of the concentration in the middle of the SML without reaction is

$$C_{NR}\left(\frac{l}{2}\right) = \frac{C_{ULW} + C_0}{2} \quad (8)$$

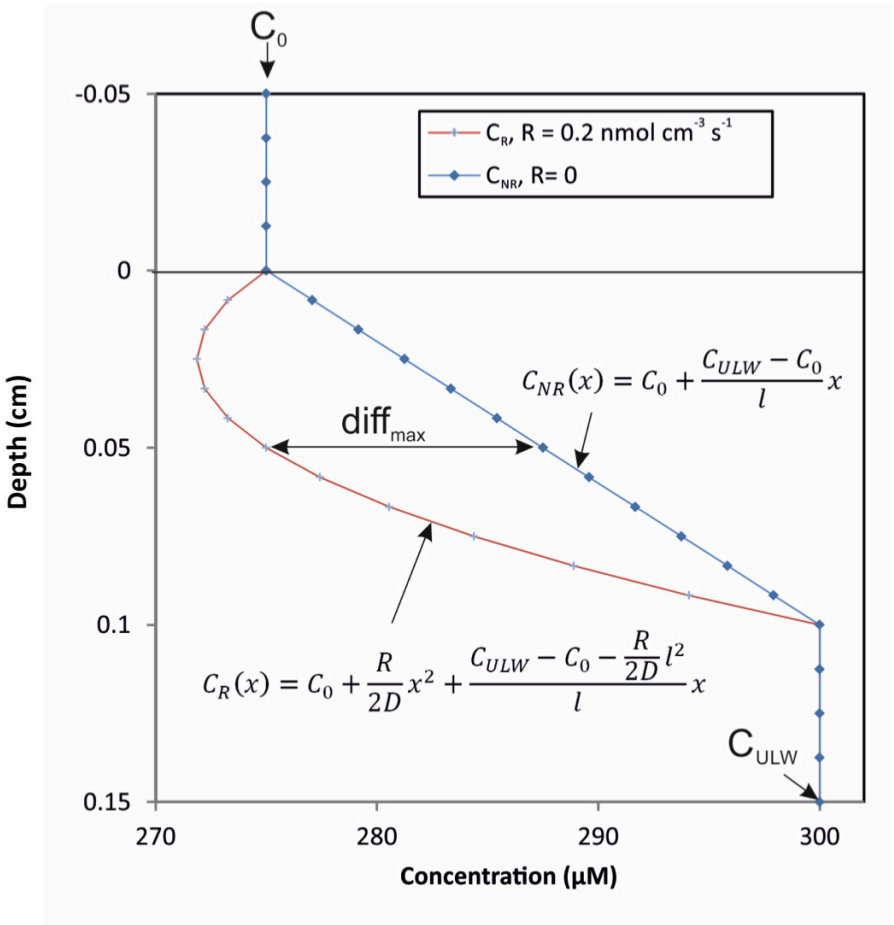

FIGURE 1 | Model of theoretical O_2-profiles across the air-water interface. The two models indicate a gradient curvature at high reaction rate (red line) vs. a straight line gradient at a reaction rate equal to zero (blue line) and the maximum absolute difference ($diff_{max}$) between the two profiles.

The maximum relative difference between the concentration profiles with and without reaction is thus

$$diff_{rel,\max} = \frac{Rl^2}{4D\,(C_{ULW} + C_0)} \quad (9)$$

Water Sampling

To sample the SML we used the glass plate technique (Harvey and Burzell, 1972), where a clean, hydrophilic glass plate is introduced vertically through the water surface until it is fully immersed. It is withdrawn at a controlled rate of 5–6 cm s^{-1} as suggested by Carlson (1982a) resulting in the adhesion of an ∼20–100 µm thick SML to the glass plate (Carlson, 1982a; Shinki et al., 2012). The thickness of the collected SML is determined by water density and viscosity, surface tension, withdrawal speed, and gravity (Levich, 1962). The SML adhering to the glass plate was scraped off into glass bottles until a volume of ∼30 mL has been collected.

While the glass plate sampling technique assumes that the majority of material collected originates from the SML, dilution with bulk water (ULW) cannot be ruled out. Wurl et al. (2011a) investigated the effect of selective adhesion of sample material to glass bottles used for sample collection. They showed that only about 10% of all organic gel-like particles from a water sample adhered to the interior of a glass bottle. Assuming that this would be equivalent to unspecific adhesion of ULW material to the glass plate after immersion into the water, only 10% of organic material in SML samples may originate from the ULW. Similar approaches to test the amount or type of microorganisms from the ULW attaching to the glass plate during SML sampling are missing. However, the glass plate technique was shown to neither quantitatively (Agogué et al., 2004) nor qualitatively (Stolle et al., 2009) select microorganisms during collection. These findings overall imply that the SML samples collected with the glass plate technique very well represent the SML with only little dilution with ULW material. Samples from the ULW were collected from 30 cm water depth with a syringe connected to a hose (**Supplementary Figure 1**). The glass plate was cleaned with 70% ethanol before one or two dips of SML sample were taken to pre-rinse the glass plate, the funnel and the collection bottle. The syringe and the bottle for ULW sample were also pre-rinsed with sample water.

Autotrophic Biomass and Quantum Yield

For the analysis of chlorophyll *a* (Chl *a*), 20–100 mL of each water sample were filtered onto glass microfiber filters (grade GF/F, Whatman, UK), stored at −20°C, and extracted in 90% acetone overnight at 4°C. Samples were analyzed at excitation wavelength 430 nm and emission >665 nm using a calibrated handheld fluorimeter (*Aqua*fluor^{TM}, Turner Designs, CA, USA). The calibration equation was derived from spinach extracts (Sigma Aldrich, Germany).

The quantum yield (Fv/Fm) of phytoplankton in the ULW was measured every 10 s with a PhytoFlash sensor (Turner Designs, CA, USA) as described in Mustaffa et al. (2017). The PhytoFlash was calibrated with a *Scenedesmus obliquus* culture. Tank water from 20 cm water depth was pumped continuously into the PhytoFlash in a closed loop. For comparison with the PAR data, mean values of the quantum yield for every 30 min were calculated.

Enumeration of Bacterial and Small Autotrophic Cells

For determination of the abundance of bacterial and small autotrophic cells, water samples were preserved with glutaraldehyde (1% final concentration), incubated for 1 h at 4°C and snap-frozen at −80°C. Prior to counting, all ULW and SML samples were pre-filtered by gravity through CellTrics® 50 μm filter (Sysmex Partec, Germany) to avoid clogging of the flow cytometer (BD Accuri C6, BD Biosciences, CA, USA). Autotrophic cell counts were determined by measuring autofluorescent emission and scattered light (Marie et al., 2000). Bacterial cells were stained and counted as described in Rahlff et al. (2017a).

In order to evaluate if the bacterial and phytoplankton microbial community in the tank was composed of representative, naturally occurring organisms, we analyzed the community composition based on 16S rRNA and 18S rRNA gene fingerprints. Details about the methods applied and the results obtained can be found in the **Supplementary Material**.

Determination of Metabolic Activity in Incubation Experiments

Duplicates of each SML and ULW sample were filled into 3-mL Exetainers® (Labco Limited, UK) and closed gas-tight without headspace. Incubation of samples was either conducted under ambient light condition (to allow for primary production and O_2 consumption) or in dark controls (to determine O_2 consumption alone). All Exetainers® were incubated in the tank at *in situ* water temperature at the respective depth (**Supplementary Figure 1**). A fixed needle-type oxygen optode (OXF500PT, Pyro Science, Germany) was used to measure O_2 concentration within the Exetainers® at the start (t_0) and end (t_{end}) of the incubation period. During 4 of 5 incubation experiments, additional intermediate measurements were done, here referred to as t_n, where n refers to the number of the intermediate measurement. The incubation period ranged from ∼3 to 49 h (**Supplementary Table 1**). The optode was calibrated each day according to the manufacturers' instructions using air-saturated water, i.e., bubbling of tank water for 15 min (100% O_2) and an anoxic 0.1 M sodium ascorbate solution (0% O_2). Using these two calibration points, the "Pyro Oxygen Logger" software (version V3.204) automatically calculates the O_2 concentration (μmol O_2 L^{-1}) based on the salinity and temperature dependence of O_2 solubility (Garcia and Gordon, 1992). The temperature was continuously recorded with a TDIP15 probe (Pyro Science, Germany).

Measurements within each Exetainer® were conducted at *in situ* temperature for at least 5 min. After stabilization of the O_2 signal, the O_2 concentration was recorded for 1.5 min, from which the mean O_2 concentration was calculated. The standard error (SE) for this determination of the mean was on average 0.33 μmol O_2 L^{-1} (Experiment 1) and 0.14 μmol O_2 L^{-1} (Experiment 2). Rates of NCP and O_2 consumption were defined as the difference in O_2 concentration between two time points in the light and dark incubations, respectively, divided by the elapsed time and are given in μmol O_2 L^{-1} h^{-1}. Error propagation of SE when subtracting two means (M1 and M2) was calculated by

$$SE\,(M1 - M2) = \sqrt{SE(M1)^2 + SE(M2)^2} \tag{10}$$

and was <0.2 μmol O_2 L^{-1} h^{-1} except for three time points (**Table 1**).

Statistical Analyses

Potential influential data in the relationships shown in **Figure 3** were defined as outliers if their Cook's distance (Cook, 1977) calculated using R version 3.4.3 (R Core Team, 2017) was >4 times the mean Cook's distance of the respective dataset. These outliers were excluded from least-square regression models used for Spearman rank correlation.

Non-parametric Spearman rank correlation analyses (two-tailed, 95% confidence interval) for changes in O_2 concentration in the ULW vs. mean PAR or NCP in SML and ULW (**Figure 3**) were performed using GraphPad Prism (Version 5.00 GraphPad Software, San Diego CA, USA). Results of the correlation analyses and identified outliers are shown in **Supplementary Table 2**.

RESULTS

O_2 Profiles at the Water Surface

High-resolution O_2 profiling using a microsensor revealed profound dynamics of O_2 profile formation across the air-water interface. **Figure 2** shows four representative shallow (<5 mm water depth) and deep profiles (<5 cm water depth) from two consecutive days of each experiment. In both experiments, profiles of dissolved O_2 revealed high vertical and temporal variability. The shallow profiles showed the formation of O_2 gradients in the uppermost water column with steadily increasing O_2 concentrations from the air-water interface to a water depth of ∼1 mm (**Figures 2A,B**). The thickness of the SML was on average 1,100 μm (±295 μm). O_2 profiles below 1.1 mm water depth showed strong vertical variability with changing O_2

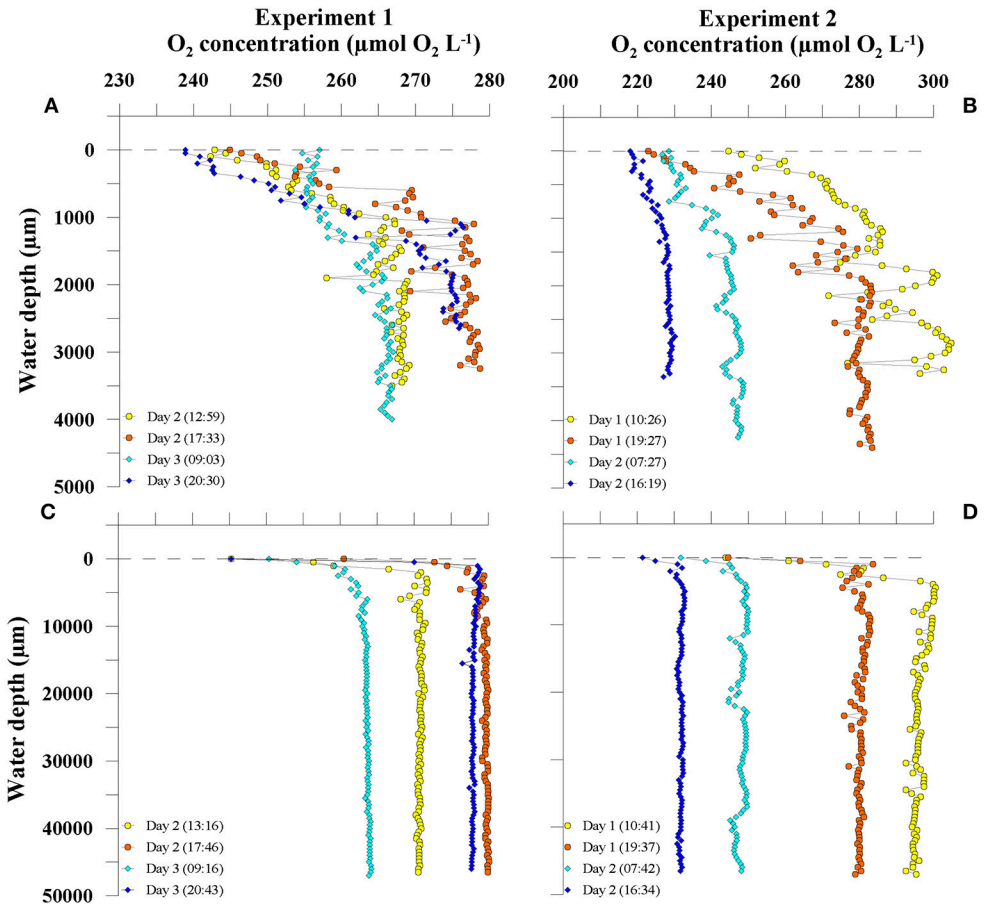

FIGURE 2 | Depth distribution of O_2 concentration in shallow **(A,B)** and deep profiles **(C,D)**. Four exemplary profiles from two consecutive days from Experiment 1 **(A,C)** and Experiment 2 **(B,D)** are shown. Time corresponds to local time (UTC + 01:00).

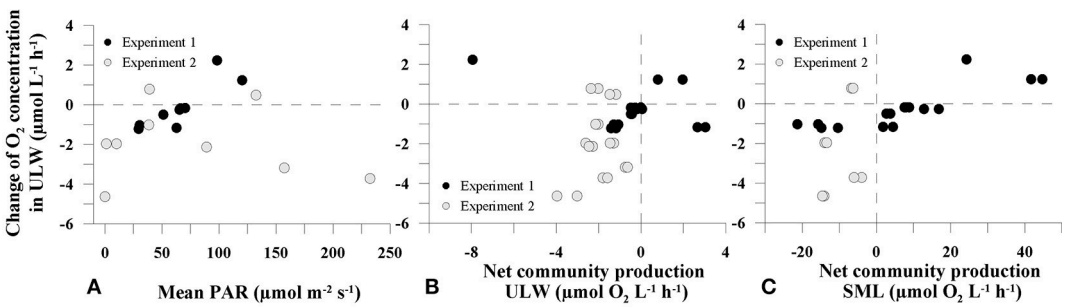

FIGURE 3 | Relationship between temporal changes of O_2 concentration in the underlying water (ULW) and mean photosynthetically active radiation (PAR) **(A)**, net community production (NCP) in ULW **(B)** and the sea-surface microlayer (SML) **(C)**.

concentration of up to 30 µmol O_2 L^{-1} within a range of 500 µm water depth (e.g., Experiment 2, Day 1, 10:26, **Figure 2B**).

From the gradients in the upper 1.1 mm we calculated diffusive rates. During Experiment 1, all rates ranged between −0.08 µmol O_2 L^{-1} h^{-1} and −0.37 µmol O_2 L^{-1} h^{-1}. The diffusive rates during Experiment 2 ranged between 0.09 µmol O_2 L^{-1} h^{-1} and −0.58 µmol O_2 L^{-1} h^{-1} (**Table 1**).

In order to assess the temporal variability of O_2 concentration in the tank water, we calculated the temporal changes in O_2 concentrations in 1.5–4 cm water depth from the deep profiles. During the first experiment, an O_2 production up to 2.2 µmol O_2 L^{-1} h^{-1} during the day and O_2 consumption up to −1.2 µmol O_2 L^{-1} h^{-1} over night was observed (**Figure 2C**, **Table 1**). In the second experiment, increases in O_2 concentration during

the day were lower (up to 0.8 μmol O_2 L^{-1} h^{-1}) compared to the first experiment, but consumption of O_2 was enhanced (up to −4.6 μmol O_2 L^{-1} h^{-1}) (**Figure 2D** and **Table 1**). In Experiment 1, the changes in O_2 concentration in the ULW between two profiles were clearly linked to PAR (Spearman's rank correlation coefficient (r_s) = 0.905, $p = 0.005$, $n = 8$, **Figure 3A** and **Supplementary Table 2**), but not in the second experiment (**Figure 3A**).

Modeling O_2 Turnover at the Air-Water Interface

Using the data from our O_2-profiles, we calculated the theoretical biological O_2-production and -consumption with a simplified profile model, in order to obtain NCP rates required to influence O_2-gradients within the DBL. We considered the DBL to be 1.1 mm thick as deduced from all O_2 gradients. Equation (9) shows that the maximum relative difference between the concentration profiles with and without biological activity (i.e., $R =$ reaction rate) increases with rising NCP rate and thicker DBL, whereas it decreases with increasing diffusion coefficient and absolute concentration levels. For an O_2 microelectrode, the relative precision is ∼1%, and the O_2 diffusion coefficient is $\sim 2 \times 10^{-5}$ cm^2 s^{-1} at 20°C and salinity of 30 as measured in the tank. Thus, to be able to distinguish between profiles with and without biological activity, if C_0 and $C_{ULW}(x)$ are e.g., 245 and 278 μmol L^{-1}, respectively (**Figure 2A**, Day 2 (17:33), we require a NCP rate such as

$$\left| \frac{Rl^2}{4D\,(C_{ULW}+C_0)} \right| > \sim 1\% \tag{11}$$

or

$$|\mathbf{R}| > \sim \mathbf{124.5\ \mu mol\ L^{-1}\ h^{-1}}. \tag{12}$$

The lowest NCP rate calculated by the model using our profile data was 103.8 μmol O_2 L^{-1} h^{-1}, implying that a NCP rate beyond ±103.8 μmol O_2 L^{-1} h^{-1} would be needed to cause detectable shifts in the O_2-gradients within the DBL of 1.1 mm thickness.

Net Community Production of Neuston and Plankton

During both experiments, light and dark incubations were performed to determine NCP and O_2 consumption rates, respectively. In both experiments, nearly all dark incubations of SML samples showed very strong O_2 consumption, causing O_2 concentration at t_{end} to be close to 0 μmol O_2 L^{-1} (**Supplementary Figure 4**). Thus, O_2 consumption rates could not be reliably determined for the present study as we could not rule out limitation of O_2 for the heterotrophs. This O_2-limitation did never occur in the NCP incubations. Consequently, only NCP rates, which were not O_2-limited at the end of the incubations, were used as a measure for metabolic activity in this study.

During both experiments, NCP showed pronounced rates in SML samples ranging between −21.3 and 44.8 μmol O_2 L^{-1} h^{-1}, indicating strong heterotrophic and autotrophic metabolism, respectively. NCP rates in the ULW fluctuated in a narrower range between −8.0 and 3.0 μmol O_2 L^{-1} h^{-1} (**Table 1**). In the first experiment, NCP dynamics were positively related to PAR (**Figure 4**) indicating a strong influence of both auto- and heterotrophic processes in the tank water. Despite high PAR values during Experiment 2, NCP rates were never positive in SML or ULW, indicating a shift toward a net heterotrophic system (**Figure 4**).

To explore whether metabolic activity of neuston and plankton, as determined by NCP rates, could explain the temporal shifts in O_2 profiles, NCP was plotted against changes in O_2 concentration in the ULW. Both NCP rates in the SML and ULW were related to changes in O_2 concentration in the tank water (**Figures 3B,C**). However, this relationship was statistically significant only for NCP rates of SML samples in Experiment 1 ($r_s = 0.820$, $p < 0.001$, $n = 15$, **Supplementary Table 2**).

Development of Auto- and Heterotrophic Communities

The abundance of auto- and heterotrophic organisms generally differed between the two experiments, and between the SML and ULW. Bacterioplankton abundance, i.e., in the ULW, decreased from 5.1×10^7 cells mL^{-1} to 3.4×10^7 cells mL^{-1} during the first experiment and slightly increased from 2.8×10^7 cells mL^{-1} to 4.1×10^7 cells mL^{-1} during the second experiment (**Figure 5A**). Bacterioneuston abundance increased from 6.0×10^7 cells mL^{-1} to 1.0×10^8 cells mL^{-1} during the first experiment and from 2.7×10^7 cells mL^{-1} to 8.8×10^7 cells mL^{-1} during the second experiment (**Figure 5A**). Thus, an enrichment of bacteria in the SML compared to the ULW was always apparent (up to 3-fold, Day 6). A single exception was Day 1 of the second experiment, where abundances in the SML were reduced by 8×10^5 cells mL^{-1} (**Figure 5A**). The abundance of small autotrophic cells (<50 μm) ranged between 2.6×10^5 and 1.6×10^6 cells mL^{-1} and showed no consistent differences between the SML and the ULW during the first experiment. During the second experiment, small autotrophic cells were generally less abundant compared to the first experiment and always depleted in the SML compared to the ULW (**Figure 5B**).

Very high Chl *a* concentrations were measured both in the SML (max: 450 μg Chl *a* L^{-1}) and the ULW (max: 14 μg Chl *a* L^{-1}) during both experiments (**Figure 5C**). Chl *a* concentration in the SML was up to 34-fold higher compared to the ULW during the first experiment. During the second experiment, Chl *a* concentration in the ULW declined while it simultaneously increased in the SML (up to 38-fold compared to the ULW), but Chl *a* concentration was overall lower compared to the first experiment. This decline in Chl *a* concentration was independent of PAR, which peaked at 874 μmol m^{-2} s^{-1} during the second experiment, indicating the shift toward a net heterotrophic system. In both experiments, high PAR values (>500 μmol m^{-2} s^{-1}) were associated with lower quantum yields in the ULW (**Supplementary Figure 5**) especially at high light intensities around noon.

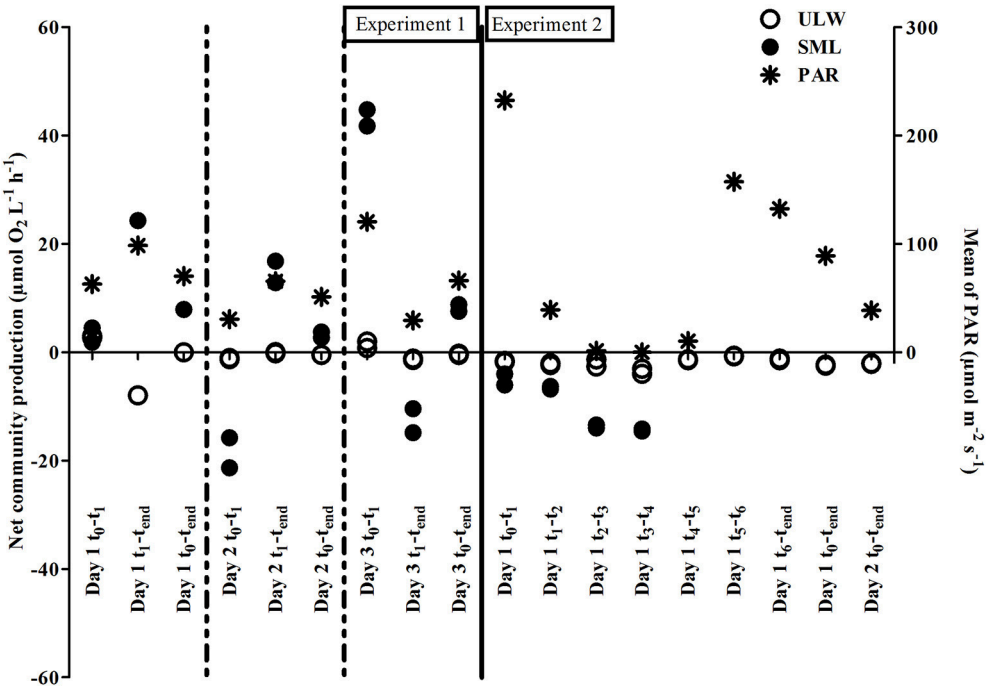

FIGURE 4 | Net community production (NCP) for the sea-surface microlayer (SML) and underlying water (ULW) and mean photosynthetically active radiation (PAR) for the two experiments.

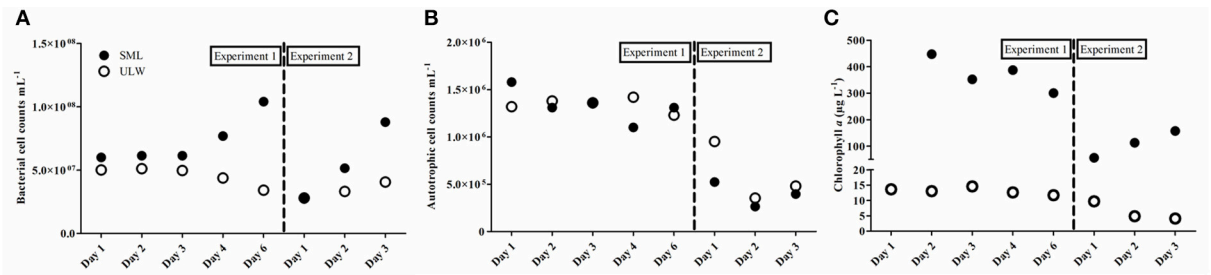

FIGURE 5 | Absolute cell abundance of bacteria **(A)**, small autotrophs **(B),** and chlorophyll *a* concentration **(C)** in the sea-surface microlayer (SML) and underlying water (ULW) for the two experiments.

DISCUSSION

Biological Effects on O_2 Profile Variability

Without any influence of chemical enhancement or biological activity, exchange processes across the air-water interface in our tank system would be solely diffusion-limited (Pereira et al., 2016). In the present study, the slope direction of O_2 gradients within the upper 1.1 mm always showed higher concentration of O_2 in water compared to air (**Figure 2**), except for the very last day, where the tank water became a sink for O_2, most likely due to the increasing effect of net heterotrophy (**Table 1**). Thus, the diffusive rates calculated from the gradients in the upper 1.1 mm were generally negative, indicating a permanent diffusion of O_2 from water to air (**Table 1**). However, the diffusive rates (mean = -0.25 ± 0.18 µmol O_2 L^{-1} h^{-1}, $n = 18$) could only insufficiently explain the temporal dynamics of changing O_2 concentration in the tank (mean = -1.02 ± 1.77 µmol O_2 L^{-1} h^{-1}, $n = 18$), suggesting that the latter was rather driven by biological O_2 production and consumption.

Net community production (NCP) rates measured in ULW (mean = -1.35 ± 2.19 µmol O_2 L^{-1} h^{-1}, $n = 18$) and SML samples (mean = 2.63 ± 17.60 µmol O_2 L^{-1} h^{-1}, $n = 13$) were generally exceeding the diffusive rates. Moreover, in the first experiment, changing O_2 concentration in the ULW seemed to be related to plankton and neuston NCP (**Figures 3B,C**). In the second experiment, the overall decreasing O_2-concentration in the ULW was accompanied by general O_2 consumption in incubated samples from the SML and the ULW (**Figures 3B,C**). Calleja et al. (2005) found planktonic metabolism in the top 2 cm of the ocean surface in the Northeast Atlantic to influence and

control direction of pCO_2 exchange but found no significant relationship for changes in pCO_2 and NCP in 5 m water depth. Making *in situ* measurements across the air-water interface, we can confirm a link between NCP and changing O_2 concentration within the upper 5 cm of the water column.

Even though biological communities influenced the temporally changing O_2 concentration in the tank, we could not find evidence for direct metabolic control of the neuston on *in situ* O_2 gradients at the air-water interface itself (**Figure 2**). For example, we did not observe distinct curvatures in the upper 1.1 mm of the O_2 gradients (i.e., DBL), which may result from O_2 production or consumption. We made this observation despite the fact that NCP of the neuston was on average 17-fold enhanced compared to the plankton. This is supported by our profile model, which shows that O_2 consumption / production in excess of 103.8 μmol L^{-1} h^{-1} within the DBL is required to measure detectable effects on O_2 gradient curvatures. However, during this experiment, the highest positive and negative NCP rates were measured in SML samples and were 44.8 μmol L^{-1} h^{-1} and −21.3 μmol L^{-1} h^{-1}, respectively, and, thus, below the threshold of ±103.8 μmol L^{-1} h^{-1} indicated by the model.

Furthermore, signal fluctuations of the profiles varied more than 1%, which was applied in the idealized model settings. These fluctuations were probably caused by microturbulence, e.g., due to buoyancy fluxes, in the DBL. Thus, the reaction rates (i.e., NCP rates) must have been even higher in this study to be detectable over the fluctuations. It is also important to note that the profile model assumes a sharp delineation between a stagnant diffusive SML and a completely mixed ULW. In reality, there will be a gradual transition between the two phases, governed by turbulent forces. This will make higher rates necessary than those indicated by the model to recognize and quantify reaction rates within the SML. Overall, our findings suggest, that any profound contribution of neuston metabolism to O_2 gas exchange across the air-water interface is unlikely.

Neuston Activity in Thick Surface Films

The O_2 gradients observed in our experimental setup indicate the formation of a thick surface film stabilizing the uppermost 1.1 mm of the water column. We observed a substantial accumulation of auto- and heterotrophic organisms in our SML samples compared to the ULW. The enrichment of bacteria in the SML is highly dependent on SML integrity (Stolle et al., 2010; Rahlff et al., 2017a), and after filling the tank, the water became increasingly settled until stagnancy, i.e., no induced mixing except microscale turbulence by buoyant fluxes and movement of the microsensors. This caused bacterial abundance to increase within the SML during both experiments (**Figure 5A**). Likewise, we observed high numbers of small autotrophs, Chl *a* concentrations of up to 38-fold in SML over ULW (**Figures 5B,C**). These enrichments have been previously observed in the field (Hardy and Apts, 1984). Nevertheless, in our study, autotrophic biomass and bacterial abundances were about one order of magnitude larger compared to the natural environment (Poremba et al., 1999; Sperling et al., 2012). Despite this very high biomass accumulation, we identified typical members of natural marine bacterial and eukaryotic communities with strong differences between the SML and ULW (**Supplementary Figures 6**, **7**). Some of the bacterial taxa belonged to the families of *Rhodobacteraceae* and *Flavobacteriaceae* (**Supplementary Table 3**), which are common SML inhabitants (Franklin et al., 2005). They were attributed to the presence of polysaccharide microgels (Taylor and Cunliffe, 2017), which strongly enrich in the SML (Wurl and Holmes, 2008). In addition, we detected an organism related to the diatom *Chaetoceros calcitrans* (**Supplementary Table 3**), which may produce large amounts of extracellular polysaccharides (Corzo et al., 2000) and, thus, could have supported the pronounced SML formation in our study.

In our experiments, the autotrophic community responded to diurnal light availability as measured by decreased quantum yields in the ULW during high light exposure around noon (**Supplementary Figure 5**). Nevertheless, the strong positive NCP rates in the SML (**Figure 4**) suggest that inhibition of photosynthetic activity by solar radiation was lower compared to field observations (Williams et al., 1986; Ignatiades, 1990) probably due to shielding by the greenhouse. We observed light-driven autotrophic O_2 production during the day and heterotrophic O_2 consumption during the night in the first experiment. In the second experiment, phosphate-limitation (as measured from a single sample on the last day of the experiment) most likely caused a decay of the autotrophic community, resulting in net heterotrophic metabolism in the tank water (**Figure 4**). NCP rates in the SML were generally higher compared to ULW (**Figure 4** and **Supplementary Figure 4**), and enhanced metabolic activity, especially of heterotrophic bacteria, is a well-known feature of the SML (Obernosterer et al., 2005; Reinthaler et al., 2008). Other studies reported SML NCP rates between −0.4 to +1.0 μmol O_2 L^{-1} h^{-1} for different coastal marine systems (Obernosterer et al., 2005; Rahlff et al., 2017b). The NCP rates in the SML of the present study (−21.3 to 44.8 μmol O_2 L^{-1} h^{-1}) are several 10-folds higher, which was most likely caused by the large number of auto- and heterotrophic microorganisms.

Overall, neuston biomass and activity was strongly enhanced in the thick surface film of our tank. In the natural environment, such films with biofilm-like properties are known as slicks (Wurl et al., 2016), and can involve high biomass, e.g., during cyanobacteria blooms (Sieburth and Conover, 1965; Wurl et al., 2018). However, our study suggests that the natural neuston community will not have significant, direct effects on O_2 gas exchange, although such thicker films limit diffusion (Wurl et al., 2016).

Implications for Gas-Exchange and Future Studies

Using microsensors, we generally observed a constant change of O_2 concentration within the uppermost 1.1 mm of the water column. This implies that the surface layer in our experimental setup had a vertical dimension of ∼1.1 mm. Zhang et al. (2003) conducted a similar microsensor study and defined the SML as a "layer of sudden change" with a thickness of ∼60 μm. Interestingly, these authors used natural seawater, which had

been pre-filtered with a pore size of 0.45 μm, thus excluding large particles and most organisms in contrast to our study. Measuring within cyanobacterial aggregates floating at the air-water interface, Ploug (2008) could show that O_2 concentration changed strongly within few millimeters depth. Thereby, gross primary production was only detectable in the uppermost 1.1 mm, which very well resembles the dimension of the thick surface film observed in our study. Thus, we consider the SML in our study to be 1.1 mm thick, following the definition of Hunter (1997), that the vertical dimension of the SML is defined by "[…] physical, chemical, or biological properties that are measurably different from those of adjacent sub-surface waters." Based on this, our profile model assumes a DBL thickness of 1.1 mm, and that metabolic activity measured in the SML samples is homogeneously distributed within the DBL. This may not be true as we have only measured NCP in the samples taken with the glass-plate, which collects the SML with ∼40–100 μm layer thickness (Carlson, 1982a). Future studies will need to unravel if metabolic activity is changing vertically within the upper millimeters of the water column.

If we assume that the high neuston NCP rates measured in our study would only affect the ULW and not the atmosphere, the small volume of the SML compared to the remaining ∼700-L tank volume would still allow for no more than 7.1% (see **Supplementary Table 4**) neuston contribution to O_2 concentration changes in the ULW. Conditions in the field would generally be more variable, and often preclude such strong accumulation of biomass in the SML except in slicks (Wurl et al., 2016). For example, cell abundances are typically enriched only at calmer sea states below ∼5 m s^{-1} (Rahlff et al., 2017a) and slicks persist until a similar wind speed threshold (Romano, 1996). Even though our study shows that microbial activity at conditions similar to slicks (i.e., low turbulence and high biomass) are insufficient to influence the exchange of oxygen, the increased thickness of the diffusion layer across slicks can reduce gas fluxes between the ocean and atmosphere (Salter et al., 2011; Wurl et al., 2016). Surfactants are hereby of special interest as they show a global distribution, are frequently enriched in the SML and slicks (Wurl et al., 2011b) and known to significantly reduce O_2 evasion rates (Frew et al., 1990). Surfactants could have played an important role in our tank due to the high biomass observed because phytoplankton and bacteria produce surfactants (Satpute et al., 2010). Due to limited SML sample volume we could only determine surfactant concentrations in a few samples, which show overall very high concentrations in the tank (2,947 ± 3,574 μg Teq L^{-1}; $n = 16$) compared to the natural environment (Ribas-Ribas et al., 2017) and 4.2-fold ± 2.3 (mean ± standard deviation, $n = 8$) enrichments within the SML (**Supplementary Table 5**). Even if we did not observe direct metabolic contributions of neuston organisms to the formation of O_2 gradients across the air-water interface, indirect influence on O_2 gas-exchange, e.g., by the organismal release of surfactants and increasing DBL thickness, cannot be excluded.

In addition, the neuston community may potentially influence the exchange of certain (trace) gases that have a low background concentration, e.g., carbon monoxide or methane (Conrad and Seiler, 1988; Upstill-Goddard et al., 2003). Whether under certain conditions, such as during extreme surface blooms of autotrophs or at sites of high organic matter availability, e.g., in aquatic foams or slicks, neuston metabolic processes could be influential for exchange processes of these trace gases, needs further investigation.

Limitations and Outlook for Future Studies

Microelectrodes have been used to investigate gradients across different marine boundary layers, e.g., sediments and microbial mats (De Beer et al., 1997), and aggregates (Ploug and Grossart, 1999). Despite the small dimensions of their tips, disturbance of the boundary layers by the introduction of microsensors has been demonstrated above marine sediment (Nøhr Glud et al., 1994). In this study, potential artifacts of the profiles measured could originate from moving the sensor through the different layers of water, and from penetrating the sensor through the water surface from the air above. Capillary forces could force the water surface to rapidly creep up the hydrophilic glass sensor tip, once the sensor tip touches the surface. This could cause a deformation of the water surface and the DBL. Such a local deformation would instantaneously raise the top of the DBL relative to the sensor tip, effectively placing the sensor tip inside the DBL. This relative shift in sensor tip position would cause a step change in the oxygen profile, both if the next data point is measured immediately and if a new diffusion steady state is awaited, which will take some tens of seconds for a 1.1 mm thick DBL (Crank, 1975). Furthermore, a deformation of the water surface in principle changes the diffusion geometry, resulting in non-linear concentration profiles inside the DBL. We could neither detect discontinuities in our oxygen profiles at the air-water interface (**Supplementary Figure 8**) nor systematic non-linearity in the DBL. Consequently, we conclude that artifacts due to disturbance of the water surface and the DBL by the microsensor play an insignificant role for our results.

Microprofiling by O_2 microsensors provides a very sensitive method for studying O_2 profiles at the air-water interface at high spatial resolution. The SML can be assumed to be at equilibrium with the atmosphere, and thus provides an internal reference point for calibration. This eliminates the errors associated with a separate calibration procedure that requires very careful temperature control relative to the experimental set-up. However, albeit their sensitivity, microsensors could not be used to quantify O_2 production and consumption rates in the SML directly during profiling, because NCP rates were relatively low compared to the O_2 background concentrations in the tank water. Assuming background concentrations to become negligible, the relative difference becomes correspondingly large (Equation 9). In this case, it is the absolute difference expressed in Equation (13), rather than the relative difference, that becomes limiting. Under favorable conditions, an O_2 sensor can have an absolute signal precision on the order of 0.1 μM near zero concentration. With a diffusion coefficient of $2 \times 10^{-5}\ cm^2\ s^{-1}$ and a DBL of 1.1 mm, detecting the activity on the profile thus requires:

$$\frac{Rl^2}{8D} > \sim 0.1\ \mu M \tag{13}$$

or

$$R > \sim 5\ \mu mol\ L^{-1}\ h^{-1} \quad (14)$$

This rate is in the same order of magnitude as many of the rates measured in this experiment. These rates could be quantified *in situ* by microprofiling through the air-water interface if the O_2 concentration in both the headspace and water phase has first been lowered artificially, e.g., by flushing with N_2. Such measurements would only be valid under the assumption that the process rates are not affected by the low concentration levels. However, this assumption seems reasonable, as values for the apparent half-saturation constant of the Michaelis-Menten equation (K_m) for microbial oceanic O_2 consumption have been shown to be in the nanomolar range (Tiano et al., 2014; Garcia-Robledo et al., 2016). Also, for compounds with a natural low ambient concentration and where a suitable microsensor exists, e.g., for nitrous oxide (N_2O), SML microprofiling can likely be used to determine reaction rates *in situ*. Applying microsensors in the field is challenging mostly because sea surface motion, i.e., waves, already exceeds the spatial measurement resolution of the sensor. Collecting natural SML samples onboard research vessels might help to approach *in situ* conditions as close as possible, but needs to consider other obstacles, e.g., the alteration of surface area of the sample, as well as onboard vibrations that interfere with sensor measurements.

CONCLUSIONS

The formation of O_2 profiles across the SML to a water depth of 5 cm was studied using microsensor technology in an experimental setup with natural seawater. Diffusive fluxes across the 1.1 mm thick DBL could not explain the temporal changes of O_2 concentration in the tank. Instead, these temporal O_2 changes were related to temporal dynamics of biological O_2 consumption and production in the tank. Thereby, we found that plankton, but not neuston metabolic activity was the main driver of O_2 gas exchange across the SML, although neuston activity may exceed plankton activity by one order of magnitude. This pilot study is the first to present measured data that direct metabolic impact by the neuston was insufficient to (a) visibly transform O_2 gradients within the SML and (b) contribute to $\geq$7.1% (see **Supplementary Table 4**) of O_2 concentration changes in the ULW. Additionally, we show that microsensors do not only offer the potential to unveil structural aspects of the SML, e.g., thickness, but can be used to unravel aspects on SML functionality. While transferability from laboratory to field proves difficult, studying O_2 profiles across the air-water boundary might further elucidate biological and physical aspects that act on gas fluxes.

AUTHOR CONTRIBUTIONS

CS and JR designed and conducted the experiments, acquired, and analyzed the data, except for cell count data, which were analyzed by H-AG. OW supervised the work and together with MR-R was involved in experimental design and data interpretation. LD contributed the model on neuston activity and to data interpretation. All authors contributed to writing, editing and discussion of the manuscript.

FUNDING

This work was supported by the European Research Council (ERC) project PASSME [grant number GA336408] and the Poul Due Jensen Foundation.

ACKNOWLEDGMENTS

We like to acknowledge our colleagues from the ICBM workshop, Uwe Ebensen, Samuel Nietzer, and Frederik Feldmann for their kind support on creating the experimental set-up. We are also grateful to Lisa Maria Engl and Mathias Wolterink for excellent technical assistance, Nur Ili Hamizah Mustaffa for surfactants measurements, Michaela Haack for sketching the experimental set-up, Andrea Gall for sharing her expertise about the fluorimeter, Thorsten Brinkhoff for providing strains for the DGGE marker, and Regina Hansen and Christian Burmeister for analyzing phytoplankton diversity and nutrients in some subsamples, respectively. This manuscript is part of a Ph.D. thesis chapter (Rahlff, 2018).

SUPPLEMENTARY MATERIAL

The Supplementary Material for this article can be found online at: https://www.frontiersin.org/articles/10.3389/fmars.2019.00011/full#supplementary-material

REFERENCES

Žutić, V., Cosović, B., Marčenko, E., Bihari, N., and Kršinić, F. (1981). Surfactant production by marine phytoplankton. *Mar. Chem.* 10, 505–520. doi: 10.1016/0304-4203(81)90004-9

Agogué, H., Casamayor, E. O., Joux, F., Obernosterer, I., Dupuy, C., Lantoine, F., et al. (2004). Comparison of samplers for the biological characterization of the sea surface microlayer. *Limnol. Oceanogr. Meth.* 2, 213–225. doi: 10.4319/lom.2004.2.213

Agogué, H., Joux, F., Obernosterer, I., and Lebaron, P. (2005). Resistance of marine bacterioneuston to solar radiation. *Appl. Environ. Microbiol.* 71, 5282–5289. doi: 10.1128/AEM.71.9.5282-5289.2005

Albright, L. J. (1980). Photosynthetic activities of phytoneuston and phytoplankton. *Can. J. Microbiol.* 26, 389–392. doi: 10.1139/m80-063

Briand, E., Pringault, O., Jacquet, S., and Torreton, J. P. (2004). The use of oxygen microprobes to measure bacterial respiration for determining bacterioplankton growth efficiency. *Limnol. Oceanogr. Meth.* 2, 406–416. doi: 10.4319/lom.2004.2.406

Calleja, M. L., Duarte, C. M., Álvarez, M., Vaquer-Sunyer, R., Agust,í, S., and Herndl, G.J. (2013). Prevalence of strong vertical CO_2 and O_2 variability in the top meters of the ocean. *Glob. Biogeochem. Cy.* 27, 941–949. doi: 10.1002/gbc.20081

Calleja, M. L., Duarte, C. M., Navarro, N., and Agustí, S. (2005). Control of air-sea CO_2 disequilibria in the subtropical NE Atlantic by planktonic metabolism

under the ocean skin. *Geophys. Res. Lett.* 32, 1–4. doi: 10.1029/2004GL022120

Carlson, D. J. (1982a). A field evaluation of plate and screen microlayer sampling techniques. *Mar. Chem.* 11, 189–208. doi: 10.1016/0304-4203(82)90015-9

Carlson, D. J. (1982b). Phytoplankton in marine surface microlayers. *Can. J. Microbiol.* 28, 1226–1234. doi: 10.1139/m82-183

Conrad, R., and Seiler, W. (1988). Influence of the surface microlayer on the flux of nonconservative trace gases (CO, H_2, CH_4, N_2O) across the ocean-atmosphere interface. *J. Atm. Chem.* 6, 83–94. doi: 10.1007/BF00048333

Cook, R. D. (1977). Detection of influential observation in linear regression. *Technometrics* 19, 15–18.

Corzo, A., Morillo, J. A., and Rodríguez, S. (2000). Production of transparent exopolymer particles (TEP) in cultures of *Chaetoceros calcitrans* under nitrogen limitation. *Aquat. Microb. Ecol.* 23, 63–72. doi: 10.3354/ame023063

Crank, J. (1975). *The Mathematics of Diffusion.* Oxford: Clarendon Press.

Cunliffe, M., Engel, A., Frka, S., Gašparovi,ć, B., Guitart, C., Murrell, J. C., et al. (2013). Sea surface microlayers: a unified physicochemical and biological perspective of the air–ocean interface. *Progr. Oceanogr.* 109, 104–116. doi: 10.1016/j.pocean.2012.08.004

Cunliffe, M., Schafer, H., Harrison, E., Cleave, S., Upstill-Goddard, R., and Murrell, J. C. (2008). Phylogenetic and functional gene analysis of the bacterial and archaeal communities associated with the surface microlayer of an estuary. *ISME J.* 2, 776–789. doi: 10.1038/ismej.2008.28

De Beer, D., Glud, A., Epping, E., and Kûhl, M. (1997). A fast-responding CO_2 microelectrode for profiling sediments, microbial mats, and biofilms. *Limnol. Oceanogr.* 42, 1590–1600. doi: 10.4319/lo.1997.42.7.1590

Eichner, M. J., Klawonn, I., Wilson, S. T., Littmann, S., Whitehouse, M. J., Church, M. J., et al. (2017). Chemical microenvironments and single-cell carbon and nitrogen uptake in field-collected colonies of *Trichodesmium* under different pCO_2. *ISME J.* 11, 1305–1317. doi: 10.1038/ismej.2017.15

Franklin, M. P., Mcdonald, I. R., Bourne, D. G., Owens, N. J. P., Upstill-Goddard, R. C., and Murrell, J. C. (2005). Bacterial diversity in the bacterioneuston (sea surface microlayer): the bacterioneuston through the looking glass. *Environ. Microbiol.* 7, 723–736. doi: 10.1111/j.1462-2920.2004.00736.x

Frew, N. (1997). "The role of organic films in air-sea gas exchange," in *The Sea Surface and Global Change,* ed R. D. Ps Liss (New York, NY: Cambridge University Press), 121–172. doi: 10.1017/CBO9780511525025.006

Frew, N. M., Goldman, J. C., Dennett, M. R., and Johnson, A. S. (1990). Impact of phytoplankton-generated surfactants on air-sea gas exchange. *J. Geophys. Res. Oceans* 95, 3337–3352. doi: 10.1029/JC095iC03p03337

Garcia, H. E., and Gordon, L. I. (1992). Oxygen solubility in seawater - better fitting equations. *Limnol. Oceanogr.* 37, 1307–1312. doi: 10.4319/lo.1992.37.6.1307

Garcia-Robledo, E., Borisov, S., Klimant, I., and Revsbech, N. P. (2016). Determination of respiration rates in water with sub-micromolar oxygen concentrations. *Front. Mar. Sci.* 3:244. doi: 10.3389/fmars.2016.00244

Gladyshev, M. (2002). *Biophysics of the Surface Microlayer of Aquatic Ecosystems*. London, UK: IWA Publishing.

Goldman, J. C., Dennett, M. R., and Frew, N. M. (1988). Surfactant effects on air-sea gas exchange under turbulent conditions. *Deep Sea Res. Part I Oceanogr. Res. Pap.* 35, 1953–1970. doi: 10.1016/0198-0149(88)90119-7

Hardy, J. T. (1973). Phytoneuston ecology of a temperate marine lagoon. *Limnol. Oceanogr.* 18, 525–533. doi: 10.4319/lo.1973.18.4.0525

Hardy, J. T. (1982). The sea surface microlayer: biology, chemistry and anthropogenic enrichment. *Progr. Oceanogr.* 11, 307–328. doi: 10.1016/0079-6611(82)90001-5

Hardy, J. T., and Apts, C. W. (1984). The sea-surface microlayer: phytoneuston productivity and effects of atmospheric particulate matter. *Mar. Biol.* 82, 293–300. doi: 10.1007/BF00392409

Harvey, G. W., and Burzell, L. A. (1972). A simple microlayer method for small samples *Limnol. Oceanogr.* 17, 156–157. doi: 10.4319/lo.1972.17.1.0156

Hunter, K. A. (1997). "Chemistry of the sea-surface microlayer," in *The Sea Surface and Global Change,* eds P. S. Liss and R. A. Duce (Cambridge: Cambridge University Press), 287–319. doi: 10.1017/CBO9780511525025.010

Ignatiades, L. (1990). Photosynthetic capacity at the surface microlayer during the mixing period. *J. Plankton Res.* 12, 851–860. doi: 10.1093/plankt/12.4.851

Levich, V. G. (1962). *Physicochemical Hydrodynamics.* Englewood Cliffs, NJ: Prentice Hall International.

Liss, P. S., and Duce, R. A. (2005). *The Sea Surface and Global Change*. Cambridge, UK: Cambridge University Press.

Marie, D., Simon, N., Guillou, L., Partensky, F., and Vaulot, D. (2000). "Flow cytometry analysis of marine picoplankton," in *In Living Color. Springer Lab Manuals,* eds R. A. Diamond and S. Demaggio (Berlin: Springer), 421–454. doi: 10.1007/978-3-642-57049-0_34

Maynard, N. G. (1968). Aquatic foams as an ecological habitat. *Zeitschrift für Allgemeine Mikrobiol.* 8, 119–126. doi: 10.1002/jobm.3630080205

Mustaffa, N. I. H., Ribas-Ribas, M., and Wurl, O. (2017). High-resolution variability of the enrichment of fluorescence dissolved organic matter in the sea surface microlayer of an upwelling region. *Elem. Sci. Anth.* 5:52. doi: 10.1525/elementa.242

Naumann, E. (1917). Beiträge zur Kenntnis des Teichnannoplanktons, I. I. Über das Neuston des Süsswassers. *Biol. Centralblatt* 37, 98–106.

Nøhr Glud, R., Gundersen, J. K., Revsbech, N. P., and Jørgensen, B. B. (1994). Effects on the benthic diffusive boundary layer imposed by microelectrodes. *Limnol. Oceanogr.* 39, 462–467. doi: 10.4319/lo.1994.39.2.0462

Obernosterer, I., Catala, P., Reinthaler, T., Herndl, G. J., and Lebaron, P. (2005). Enhanced heterotrophic activity in the surface microlayer of the Mediterranean Sea. *Aquat. Microb. Ecol.* 39, 293–302. doi: 10.3354/ame039293

Pereira, R., Schneider-Zapp, K., and Upstill-Goddard, R. (2016). Surfactant control of gas transfer velocity along an offshore coastal transect: results from a laboratory gas exchange tank. *Biogeosciences* 13, 3981–3989. doi: 10.5194/bg-13-3981-2016

Ploug, H. (2008). Cyanobacterial surface blooms formed by *Aphanizomenon* sp. and *Nodularia spumigena* in the Baltic Sea: small-scale fluxes, pH, and oxygen microenvironments. *Limnol. Oceanogr.* 53, 914–921. doi: 10.4319/lo.2008.53.3.0914

Ploug, H., and Grossart, H. P. (1999). Bacterial production and respiration in suspended aggregates - a matter of the incubation method. *Aquat. Microb. Ecol.* 20, 21–29. doi: 10.3354/ame020021

Poremba, K., Tillmann, U., and Hesse, K.-J. (1999). Distribution patterns of bacterioplankton and chlorophyll-a in the German Wadden Sea. *Helgoland Mar. Res.* 53, 28–35. doi: 10.1007/PL00012135

R Core Team (2017). *R: A Language and Environment for Statistical Computing.* , Vienna: R Foundation for Statistical Computing.

Rahlff, J. (2018). *The Role of Microbial Communities at the Sea Surface in Air-Sea Gas Exchange.* Ph.D. thesis, Carl von Ossietzky University Oldenburg.

Rahlff, J., Stolle, C., Giebel, H. A., Brinkhoff, T., Ribas-Ribas, M., Hodapp, D., et al. (2017a). High wind speeds prevent formation of a distinct bacterioneuston community in the sea-surface microlayer. *FEMS Microbiol. Ecol.* 93, 1–14. doi: 10.1093/femsec/fix041

Rahlff, J., Stolle, C., and Wurl, O. (2017b). SISI: a new device for *in situ* incubations at the ocean surface. *J. Mar. Sci. Eng.* 5:46. doi: 10.3390/jmse5040046

Ramsing, N., and Gundersen, J. (2000). *Seawater and Gases: Tabulated Physical Parameters of Interest to People Working With Microsensors in Marine Systems*. Available online at: http://www.unisense.com. (Accessed November 1, 2017).

Reinthaler, T., Sintes, E., and Herndl, G. J. (2008). Dissolved organic matter and bacterial production and respiration in the sea-surface microlayer of the open Atlantic and the western Mediterranean Sea. *Limnol. Oceanogr.* 53, 122–136. doi: 10.4319/lo.2008.53.1.0122

Revsbech, N. P. (1989). An oxygen microsensor with a guard cathode. *Limnol. Oceanogr.* 34, 474–478. doi: 10.4319/lo.1989.34.2.0474

Revsbech, N. P., and Jørgensen, B. B. (1986). "Microelectrodes: their use in microbial ecology," in *Advances in Microbial Ecology,* ed K. Marshall (New York, NY: Springer), 293–352. doi: 10.1007/978-1-4757-0611-6_7

Revsbech, N. P., Jorgensen, B. B., Blackburn, T. H., and Cohen, Y. (1983). Microelectrode studies of the photosynthesis and O_2, H_2S, and pH profiles of a microbial mat. *Limnol. Oceanogr.* 28, 1062–1074. doi: 10.4319/lo.1983.28.6.1062

Ribas-Ribas, M., Mustaffa, N. I. H., Rahlff, J., Stolle, C., and Wurl, O. (2017). Sea Surface Scanner (S3): a catamaran for high-resolution measurements of biogeochemical properties of the sea surface microlayer. *J. Atmos. Ocean Technol.* 34, 1433–1448. doi: 10.1175/JTECH-D-17-0017.1

Romano, J. C. (1996). Sea-surface slick occurrence in the open sea (Mediterranean, Red Sea, Indian Ocean) in relation to wind speed. *Deep Sea Res. Pt. I* 43, 411–423. doi: 10.1016/0967-0637(96)00024-6

Sabbaghzadeh, B., Upstill-Goddard, R., Beale, R., Pereira, R., and Nightingale, P. (2017). The Atlantic Ocean surface microlayer from 50° N to 50° S is ubiquitously enriched in surfactants at wind speeds up to 13 m s^{-1}. *Geophys. Res. Lett.* 44, 2852–2858. doi: 10.1002/2017GL072988

Salter, M., Upstill-Goddard, R., Nightingale, P., Archer, S., Blomquist, B., Ho, D., et al. (2011). Impact of an artificial surfactant release on air-sea gas fluxes during Deep Ocean Gas Exchange Experiment II. *J. Geophys. Res. Oceans* 116, 1–9. doi: 10.1029/2011JC007023

Santos, A. L., Baptista, I., Lopes, S., Henriques, I., Gomes, N. C., Almeida, A., et al. (2012). The UV responses of bacterioneuston and bacterioplankton isolates depend on the physiological condition and involve a metabolic shift. *FEMS Microbiol. Ecol.* 80, 646–658. doi: 10.1111/j.1574-6941.2012.01336.x

Satpute, S. K., Banat, I. M., Dhakephalkar, P. K., Banpurkar, A. G., and Chopade, B. A. (2010). Biosurfactants, bioemulsifiers and exopolysaccharides from marine microorganisms. *Biotechnol Adv.* 28, 436–450. doi: 10.1016/j.biotechadv.2010.02.006

Shinki, M., Wendeberg, M., Vagle, S., Cullen, J. T., and Hore, D. K. (2012). Characterization of adsorbed microlayer thickness on an oceanic glass plate sampler. *Limnol. Oceanogr. Meth.* 10, 728–735. doi: 10.4319/lom.2012.10.728

Sieburth, J. M. (1983). "Microbiological and organic-chemical processes in the surface and mixed layers," in *Air–Sea Exchange of Gases and Particles,* ed P. S. Liss, W. G. N. Slinn (Hingham, MA: Reidel Publishers Co.), 121–172. doi: 10.1007/978-94-009-7169-1_3

Sieburth, J. M., and Conover, J. T. (1965). Slicks associated with *Trichodesmium* blooms in the Sargasso Sea. *Nature* 205, 830–831. doi: 10.1038/205830b0

Sperling, M., Giebel, H.-A., Rink, B., Grayek, S., Staneva, J., Stanev, E., et al. (2012). Differential effects of hydrographic and biogeochemical properties on the SAR11 clade and Roseobacter RCA cluster in the North Sea. *Aquat. Microb. Ecol.* 67, 25–34. doi: 10.3354/ame01580

Stolle, C., Labrenz, M., Meeske, C., and Jürgens, K. (2011). Bacterioneuston community structure in the southern Baltic sea and its dependence on meteorological conditions. *Appl. Environ. Microbiol.* 77, 3726–3733. doi: 10.1128/AEM.00042-11

Stolle, C., Nagel, K., Labrenz, M., and Jürgens, K. (2009). Bacterial activity in the sea-surface microlayer: *in situ* investigations in the Baltic Sea and the influence of sampling devices. *Aquat. Microb. Ecol.* 58, 67–78. doi: 10.3354/ame01351

Stolle, C., Nagel, K., Labrenz, M., and Jürgens, K. (2010). Succession of the sea-surface microlayer in the coastal Baltic Sea under natural and experimentally induced low-wind conditions. *Biogeosciences* 7, 2975–2988. doi: 10.5194/bg-7-2975-2010

Taylor, J. D., and Cunliffe, M. (2017). Coastal bacterioplankton community response to diatom-derived polysaccharide microgels. *Environ. Microbiol. Rep.* 9, 151–157. doi: 10.1111/1758-2229.12513

Tiano, L., Garcia-Robledo, E., and Revsbech, N. P. (2014). A new highly sensitive method to assess respiration rates and kinetics of natural planktonic communities by use of the switchable trace oxygen sensor and reduced oxygen concentrations. *PloS ONE* 9:e105399. doi: 10.1371/journal.pone.0105399

Upstill-Goddard, R. C., Frost, T., Henry, G. R., Franklin, M., Murrell, J. C., and Owens, N. J. P. (2003). Bacterioneuston control of air-water methane exchange determined with a laboratory gas exchange tank. *Glob. Biogeochem. Cy.* 17, 1–15. doi: 10.1029/2003GB002043

Williams, P. M., Carlucci, A. F., Henrichs, S. M., Van Vleet, E. S., Horrigan, S. G., Reid, F. M. H., et al. (1986). Chemical and microbiological studies of sea-surface films in the Southern Gulf of California and off the West Coast of Baja California. *Mar. Chem.* 19, 17–98. doi: 10.1016/0304-4203(86)90033-2

Wurl, O., Bird, K., Cunliffe, M., Landing, W. M., Miller, U., Mustaffa, N. I. H., et al. (2018). Warming and Inhibition of Salinization at the Ocean's Surface by Cyanobacteria. *Geophys. Res. Lett.* 45, 4230–4237. doi: 10.1029/2018GL077946

Wurl, O., Ekau, W., Landing, W. M., and Zappa, C. J. (2017). Sea surface microlayer in a changing ocean – A perspective. *Elem. Sci. Anth.* 5:31. doi: 10.1525/elementa.228

Wurl, O., and Holmes, M. (2008). The gelatinous nature of the sea-surface microlayer. *Mar. Chem.* 110, 89–97. doi: 10.1016/j.marchem.2008.02.009

Wurl, O., Miller, L., and Vagle, S. (2011a). Production and fate of transparent exopolymer particles in the ocean. *J. Geophys. Res. Oceans* 116, 1–16. doi: 10.1029/2011JC007342

Wurl, O., Stolle, C., Van Thuoc, C., The Thu, P., and Mari, X. (2016). Biofilm-like properties of the sea surface and predicted effects on air–sea CO_2 exchange. *Progr. Oceanogr.* 144, 15–24. doi: 10.1016/j.pocean.2016.03.002

Wurl, O., Wurl, E., Miller, L., Johnson, K., and Vagle, S. (2011b). Formation and global distribution of sea-surface microlayers. *Biogeosciences* 8, 121–135. doi: 10.5194/bg-8-121-2011

Zhang, Z. B., Cai, W. J., Liu, L. S., Liu, C. Y., and Chen, F. Z. (2003). Direct determination of thickness of sea surface microlayer using a pH microelectrode at original location. *Sci. China Ser. B* 46, 339–351. doi: 10.1360/02yb0192

Conflict of Interest Statement: The authors declare that the research was conducted in the absence of any commercial or financial relationships that could be construed as a potential conflict of interest.

Copyright © 2019 Rahlff, Stolle, Giebel, Ribas-Ribas, Damgaard and Wurl. This is an open-access article distributed under the terms of the Creative Commons Attribution License (CC BY). The use, distribution or reproduction in other forums is permitted, provided the original author(s) and the copyright owner(s) are credited and that the original publication in this journal is cited, in accordance with accepted academic practice. No use, distribution or reproduction is permitted which does not comply with these terms.